Harmonics Measurement With a Modulated Sliding Discrete Fourier Transform Algorithm

Carlos M. Orallo, Ignacio Carugati, Sebastian Maestri, Patricio G. Donato, Daniel Carrica, *Senior Member, IEEE*, and Mario Benedetti

***Abstract*— Accurate harmonics estimation has become a key issue in power quality assessment. This paper deals with a discrete Fourier transform (DFT)-based measurement technique, which can be easily employed to accurately determine the harmonic components of a distorted signal, i.e., voltage or current. The proposed method is based on a modulated sliding DFT algorithm, which is unconditionally stable and does not accumulate errors due to finite precision representation, and a variable sampling period technique (VSPT) to achieve a frequency adaptive mechanism. It is worth noting that the VSPT changes the sampling period for a variable grid frequency condition, leading to a constant sampling frequency under steady-state conditions. The proposed method provides: 1) high degree of accuracy; 2) structural/performance robustness; and 3) frequency adaptability. Given the modular nature of the method, it is implemented on a field programmable gate array. Simulations and experimental tests are shown to verify the performance of the proposed method.**

***Index Terms*— DFT, FPGA, harmonics measurement, power quality, signal processing, variable sampling period.**

I. Introduction

With the widespread applications of advanced power electric technologies, such as switching power supplies and adjustable speed motor drives, among others, harmonic currents are increasingly being injected into power systems causing power quality degradation. Harmonics increase power system losses, damages sensitive loads, causes excessive heating in rotating machinery, creates significant interference on communication systems, and generates noise in regulating devices and control systems. In addition, the system frequency may deviate from its nominal value due to power imbalance between generation and load demand. Therefore, measuring grid harmonics, in an accurate and efficient manner, has turned into a major challenge [1]–[3].

Discrete Fourier transform (DFT) is the most widely used algorithm for harmonics measurement. DFT is widely applied for its simplicity, and it can be efficiently calculated using fast Fourier transform (FFT). By transforming the measured signal from the time domain to the frequency domain, FFT can precisely track harmonic components. However, the harmonic level and the fundamental frequency in the power system is usually time varying; especially, in long weak distribution lines, the direct application of the FFT technique for spectral analysis may lead to inaccuracies due to the leakage and picket–fence effects [4]. The leakage error is categorized into two components: short range and long range leakage errors [5], [6]. Despite the fact that several techniques can be adopted to resolve the pitfalls of FFT applications, additional computational burden could be introduced and accuracy is compromised [7]–[11].

Regarding power quality measurement, the IEC electromagnetic compatibility standard limits the number of harmonics to be considered [12], [13]. The standard requires spectrum analysis only for the first 40 harmonics, so other algorithms can be used, like the recursive algorithms of DFT [14], so-called sliding DFT (SDFT), the Goertzel transform (GT) and the sliding GT (SGT) [14], [15]. These methods detect the desired harmonics in an efficient way, save computational effort, and simplify implementation complexity. As attractive as these techniques may seem, they suffer from stability problems given the finite word length precision along with the pitfalls related to the time-varying nature of the processed signal.

Techniques for measuring harmonics are not limited to those based on Fourier analysis. Several other approaches are also effective to carry out said study. The Kalman filter, for instance, is a recursive estimation method, based on a state-space model for each new input signal sample, making it suitable for real time processing. In addition, Kalman filters are suitable for nonstationary signal analysis [16]–[18]. However, a clear disadvantage of the Kalman filter is that it requires that the information about the frequency of the power signal be specified in advance [1], [19]. Thus, a large variation in the power signal frequency could limit the use of Kalman filters. In addition, issues concerning stability and convergence are associated with the technique.

The recursive least squares (RLS) is an algorithm which recursively finds the coefficients that minimize a weighted linear least squares cost function relating to the input signals. This stands in opposition to other algorithms, such as the least mean squares (LMS) that aim to reduce the mean square error. For RLS algorithm, input signals are considered deterministic, while for LMS and similar algorithms, they are considered stochastic. RLS algorithms are widely used to accurately estimate the amplitude and phase of fundamental and harmonics components of a signal, provided that the fundamental frequency is known a priori. When compared

Manuscript received May 3, 2013; revised September 23, 2013; accepted September 24, 2013. Date of publication November 5, 2013; date of current version March 6, 2014. This work was supported by the Consejo Nacional de Investigaciones Científicas y Técnicas, Argentina, by the Universidad Nacional de Mar del Plata, Argentina, by the Ministerio de Ciencia, Tecnología e Innovación Productiva, Argentina and the Agencia Nacional de Promoción Científica y Tecnológica, Argentina. The Associate Editor coordinating the review process was Dr. Dario Petri.

The authors are with the Universidad Nacional de Mar del Plata, Conicet, Buenos Aires 7600, Argentina (e-mail: orallo@fi.mdp.edu.ar; icarugati@fi.mdp.edu.ar; somaestri@fi.mdp.edu.ar; donatopg@fi.mdp.edu.ar).

Digital Object Identifier 10.1109/TIM.2013.2287801

with most of its competitors, RLS exhibits extremely fast convergence. However, this benefit comes at the expense of high computational complexity [20], [21].

More advanced control and signal-processing techniques, including fuzzy-logic control [22], neural-network theory [23], [24], rotational invariance technique (ESPRIT) [25], [26], and adaptive signal processing [27], have also been applied. Most of these algorithms are accurate and feature a good dynamic response, still they require large amount of calculation; and, under frequency varying environments, performance gets compromised.

This paper presents a new harmonic measurement method which employs the mSDFT algorithm to attain measurement accuracy and overcome finite word length precision problems. The mSDFT algorithm uses DFT modulation properties to eliminate problems arising from finite word length precision [28]. Given the spectral leakage and picket–fence effects associated with the fundamental frequency variation and improperly selected sampling time window, a frequency adaptive mechanism is adopted. The variable sampling period technique (VSPT), postulated by the authors in previous works, is adapted to dynamically adjust the sampling period to exactly N times the fundamental frequency, and; hence, avoid the above-mentioned problems. Even though the technique is named as variable, the sampling frequency varies only during transients due to the variation of the grid frequency. Once a steady state is reached, the sampling rate remains fixed. The structural and mathematical simplicity of the mSDFT algorithm and VSPT renders it suitable for its implementation in a hardware programmable platform.

II. mSDFT Algorithm

This section provides a brief summary of the SDFT properties necessary to derive mSDFT. SDFT is a recursive algorithm implemented as an IIR filter that calculates a single value of DFT, in other words, the term k of an N-points DFT.

Let us consider a time signal $x(t)$ that is sampled at the rate $f_s = N \times f_L$ [where f_L is the frequency of $x(t)$] to produce the time sequence $x(n)$, such that $x(n) = 0$ for $n < 0$. A recursive formula for computing the DFT of the kth-bin coefficient in the time window of length N sliding along the last values of the signal $x(n)$ can be written as [14], [29], [30]

$$X_k(n) = W_N^k[X_k(n-1) - x(n-N) + x(n)] \tag{1}$$

where $X_k(n)$ is the current value of the desired spectral component, $X_k(n-1)$ is the previous value, $x(n)$ and $x(n-N)$ are samples of the input signal in the nth and $(n-N)$th time instant respectively, and $W_N = e^{j2\pi/N}$ is known as the complex twiddle factor. In this notation, the superscript k refers to the desired DFT frequency index (kth-bin), and n is a time index. Notice that (1) must be normalized by N to obtain a proper representation of the kth-bin.

The principle used for SDFT is known as the DFT shifting theorem, or the circular shift property. The value of this process in computing real time spectra is that the calculation of $X_k(n)$ is done by phase shifting the sum of the previous $X_k(n-1)$ with the difference between the $x(n)$ and $x(n-N)$ samples. SDFT is computationally efficient since a sliding window (SW) is used to compute a new DFT bin from the results of the previous DFT. So that, after obtaining the value of coefficient $X_k(n-1)$, the calculations necessary to obtain $X_k(n)$ are constant and do not depend on N.

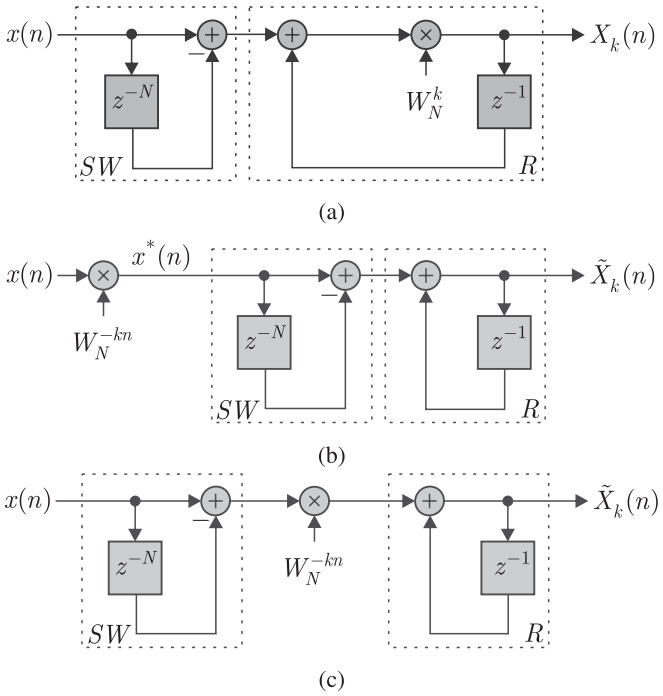

Fig. 1. (a) SDFT structure in (1). (b) Modulated SDFT structure in (4). (c) Modulated SDFT structure in (12). SW: sliding window. R: resonator.

Fig. 1(a) shows the single-bin SDFT algorithm implemented as an IIR filter. Two parts can be differentiated: the SW and the complex resonator (R) which provides the current coefficient of the kth component of the signal spectrum. The z-domain transfer function for the kth-bin of the SDFT is

$$H_{\text{SDFT}}(z) = \frac{X_k(z)}{x(z)} = \frac{W_N^k\left(1 - z^{-N}\right)}{1 - W_N^k z^{-1}}. \tag{2}$$

SDFT decreases the computational complexity of each successive N-point output on a sample-by-sample basis, if compared to DFT or FFT, but it suffers from accumulated errors and potential instabilities. The nonideal numerical precision of the coefficient W_N^k places the singularities (i.e., the poles and zeros of the transfer function) either slightly inside or slightly outside the unit circle [31]. To achieve stability, a damping factor must be included [30]. Even though this damping factor allows to achieve stability, a small error is induced in an X_k output sample, which accumulates with each new spectral component computation.

For the special case when $k = 0$ (dc component estimation), (1) takes the following form:

$$X_0(n) = [X_0(n-1) - x(n-N) + x(n)]. \tag{3}$$

The computation of successive values of $X_0(n)$ requires simple additions of the input samples in the sliding time window of length N. Owing to the absence of the typically imprecise W_N^k coefficient, the recurrence in (3) is unconditionally stable and does not accumulate errors. The modulated SDFT (mSDFT) is

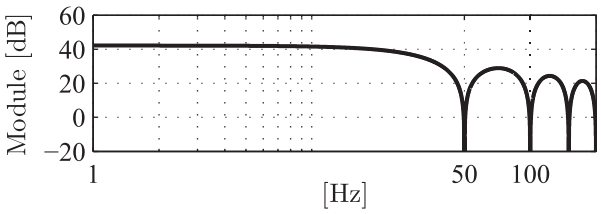

Fig. 2. Frequency response of the digital notch filter in (6), tuned with $N = 128$ for a $f_L = 50$ Hz.

an algorithm which exploits the advantages of this particular case for any k-bin [28].

The modulated SDFT is a DFT-based algorithm guaranteed to be stable without sacrificing accuracy. This algorithm uses the DFT modulation property for the chosen DFT bin with index k to effectively shift that bin to the position $k = 0$. This approach allows excluding the complex twiddle factor from the feedback loop (or resonator) and avoids accumulated errors and potential instabilities. The X_k DFT bin may be shifted to the index $k = 0$ by the multiplication of the input signal $x(n)$ by the modulation sequence W_N^{-kn}

$$\tilde{X}_k(n) = \tilde{X}_k(n-1) - x(n-N)W_N^{-k(n-N)} + x(n)W_N^{-kn}. \quad (4)$$

There is a phase difference, equal to W_N^{-k}, between the DFT bin calculated by (1) and the one obtained from (4) ($\tilde{X}_k(n)$). In [28] is shown how this difference can be corrected, but since in spectrum analysis applications only the results of the DFT magnitude are required, the correction is not needed.

The structure of the mSDFT in (4) is shown in Fig. 1(b). As there is no complex twiddle factor in the resonator, the singularities of mSDFT are located exactly (with no finite-precision numerical error) on the unit circle. Therefore, the accumulated errors and potential instabilities inherent of traditional SDFT algorithms are drastically reduced in the mSDFT. In addition, the finite precision of the twiddle factor representation is no longer a problem due to its removal from the feedback loop (R).

A z-domain transfer function for the kth-bin can be obtained by separating the effects of the modulation property in an auxiliary complex variable ($x^*(n)$)

$$x^*(n) = x(n)W_N^{-kn}. \quad (5)$$

In (5), the chosen DFT bin with index k is shifted to the position $k = 0$. Once this takes place, the transfer function from x^* to X_k becomes

$$H_{\mathrm{DNF}}(z) = \frac{\tilde{X}_k(z)}{x^*(z)} = \frac{1 - z^{-N}}{1 - z^{-1}}. \quad (6)$$

Equation (6) corresponds to a digital notch filter that rejects all the frequency multiples of f_s/N. Since $f_s = N \times f_L$, the resulting transfer function has zeros in all multiples of the input frequency (Fig. 2).

To compute the mSDFT algorithm, it is necessary to use the Euler relation to transform the twiddle factor in (5) into its real and imaginary components. By so doing, the complex twiddle factor is transformed into a periodic modulated sequence of N values

$$x^*(n) = x(n)\cos(\varphi_m(n)) - jx(n)\sin(\varphi_m(n)) \quad (7)$$

TABLE I
SINGLE-BIN DFT COMPARISON

DFT-based Algorithm	Single X_n^k Computation		Next X_{n+1}^k Computation	
	Real Multiplications	Real Additions	Real Multiplications	Real Additions
SDFT	$4N$	$4N$	4	4
GT	$N+2$	$2N+1$	$N+2$	$2N+1$
SGT	$N+2$	$3N+1$	3	4
mSDFT	$2N$	$3N$	2	3

where the phase of the modulated sequence is

$$\varphi_m(n) = \frac{2\pi nk}{N}. \quad (8)$$

Therefore, the real and imaginary components of the mSDFT for the kth-bin take the following form:

$$\mathrm{Re}\{\tilde{X}_k(n)\} = \mathrm{Re}\{\tilde{X}_k(n-1)\} + \mathrm{Re}\{x^*(n)\} - \mathrm{Re}\{x^*(n-N)\} \quad (9)$$

$$\mathrm{Im}\{\tilde{X}_k(n)\} = \mathrm{Im}\{\tilde{X}_k(n-1)\} + \mathrm{Im}\{x^*(n)\} - \mathrm{Im}\{x^*(n-N)\} \quad (10)$$

and the expression of the magnitude is as follows:

$$V_k(n) = \frac{1}{N}\sqrt{\mathrm{Re}\,[X_k\,(n)]^2 + \mathrm{Im}\,[X_k\,(n)]^2} \quad (11)$$

where V_k is the amplitude of the kth-bin. Notice normalization by N due to the low-frequency gain of the transfer function shown in Fig. 2.

If multiple DFT frequency bins have to be computed, one length-N delay buffer is needed for each frequency bin. However, due to the periodicity of W_N^{-kn}, as shown in [28], (4) can be rewritten as:

$$\tilde{X}_k(n) = \tilde{X}_k(n-1) + W_N^{-kn}[-x(n-N) + x(n)]. \quad (12)$$

Irrespective of multiple DFT frequency bins are to be computed, (12) turns into a more efficient approach as only one length-N delay buffer is needed [Fig. 1(c)]. Also, in this case, SW processes real values ($x(n)$) rather than complex ones ($x^*(n)$) as in the filter implementation of (4) shown in Fig. 1(b). These two characteristics explain the significant reduction obtained in the computational complexity when mSDFT is implemented in this manner.

Another advantage of mSDFT is the reduced number of operations needed to calculate the desired bin. A single-bin DFT computational comparison, for real only inputs, is provided in Table I. Once the first N data set are computed, the computational effort in the mSDFT algorithm is significantly reduced. When compared with other techniques for real time processing, mSDFT requires fewer multiplications and additions than SDFT, the traditional GT, and SGT do.

The mSDFT algorithm allows to measure the desired k-bin of an N sample DFT with no stability problems and accumulated errors, given its finite word length precision. Nevertheless, mSDFT faces some of the typical problems DFT does. Considering the spectral leakage and picket–fence effects related to the system fundamental frequency variation and improperly selected sampling time window, a direct application of the DFT algorithm with a constant sampling rate may lead to inaccurate results for continuously measuring

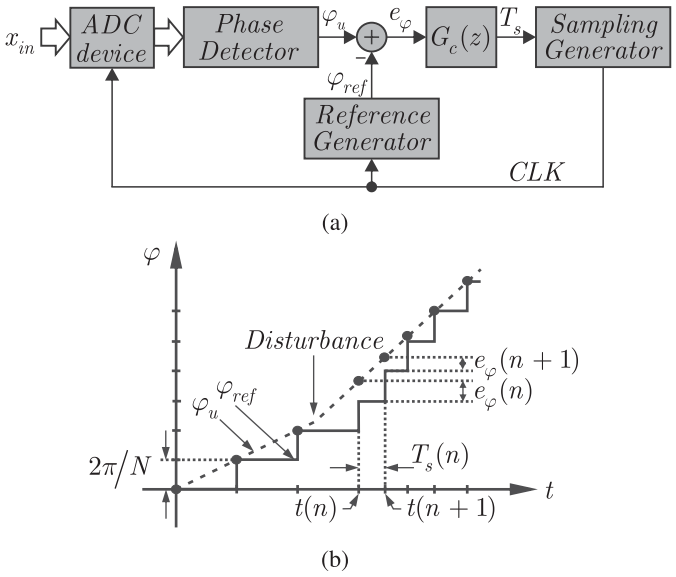

Fig. 3. (a) Variable sampling period technique (VSPT) scheme. (b) Phase error and period adjustment.

harmonics. To overcome this drawback, this paper proposes the application of a VSPT, to dynamically adjust the sampling frequency to be equal to $N \times f_L$.

III. Variable Sampling Period Technique

Previous works by the authors have proposed some synchronization methods based on a VSPT, which allows to adapt the sampling frequency to be N times the grid frequency [32]–[34]. This technique has been proven to be efficient in three-phase as well as in single-phase applications to obtain a robust synchronization mechanism, where its effectiveness was tested under different conditions and scenarios, yielding great results.

Fig. 3(a) illustrates the basic scheme for VSPT implementation. Provided the phase detector can be modeled as a transformation without dynamic, this scheme is valid both for three-phase and single-phase applications. The operating principle is based on the dynamic adjustment of the sampling frequency. The input signal is sampled and the input phase ($\varphi_u(n)$) is extracted by the phase detector. Concomitantly with the input sampling, a signal termed reference phase, is generated

$$\varphi_{\text{ref}}(n) = \frac{2\pi n}{N}. \tag{13}$$

The method relies on sampling period modification, so as to achieve a null error signal ($e_\varphi(n)$) between $\varphi_{\text{ref}}(n)$ and $\varphi_u(n)$. This is achieved by varying the sampling period $T_s(n)$ as a function of the phase error.

Fig. 3(b) shows $\varphi_{\text{ref}}(n)$ and $\varphi_u(n)$ during consecutive sampling instants. To attain synchronization, the sampling period $T_s(n)$ should be varied until the difference between the phases becomes null. Any change in the phase or frequency of the grid is reflected in $\varphi_u(n)$, and, therefore, the error between $\varphi_{\text{ref}}(n)$ and $\varphi_u(n)$ is different from zero. As illustrated in the figure, the phase error in n is reduced in $n+1$ by the sampling frequency variation. In this way, the method automatically adjusts the sampling frequency to a new value, so as to maintain a null error between $\varphi_{\text{ref}}(n)$ and $\varphi_u(n)$.

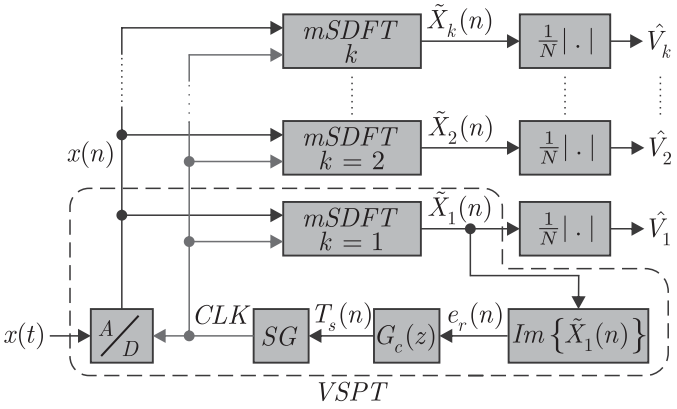

Fig. 4. Generic scheme of the proposed method (where "SG" stands for sampling generator).

Notice that the sampling frequency varies only during transients produced by changes in the grid frequency. Hence, for steady-state conditions ($e_\varphi(n) = 0$), the sampling frequency remains constant ($f_s = N \times f_L$).

In the particular case of this paper, the VSPT technique is used to dynamically adjust the sampling frequency to N times the grid frequency. This adjustment allows to avoid the spectral leakage and picket–fence effects, well known problems confronted by DFT-based algorithms, such as mSDFT.

IV. Proposed Method

This section presents a novel harmonics measurement method for applications in power systems, based on the mSDFT algorithm and VSPT. The mSDFT algorithm allows in implementing an efficient and precise harmonics measurement system, without finite word length or stability issues. VSPT is used to dynamically adjust the sampling frequency to N times the grid frequency. Such adjustment allows in avoiding the typical problems encountered by DFT-based algorithms, such as spectral leakage and picket–fence effects.

A generic layout for the proposed method is shown in Fig. 4. The elements bound by the dashed line are VSPT subsystem for frequency adjustment. This one is composed by an analog-to-digital converter (A/D), a sampling generator (SG), a controller ($G_c(z)$) and an mSDFT tuned with $k = 1$. The basic operating principle of this subsystem is as follows: in each clock pulse (CLK) the A/D acquires $x(t)$ and delivers the grid instant value ($x(n)$). This value is processed sample by sample by mSDFT (tuned with $k = 1$), delivering the instantaneous value of the fundamental spectral component ($\tilde{X}_1(n)$). A system error signal ($e_r(n)$) proportional to the phase error ($e_\varphi(n)$) can be obtained from the imaginary component of $\tilde{X}_1(n)$, as proven below. With the current $e_\varphi(n)$ value the controller can adjust the following sampling period $T_s(n)$. Then, SG block generates the CLK signal needed to trigger the A/D and to increment the instant values of every twiddle factor. The rest of the system consists in several mSDFTs and absolute value calculations, as harmonics have to

be measured. Each mSDFT simultaneously receives the $x(n)$ value and the CLK signal, and delivers the desired $\tilde{X}_k(n)$. Then, the absolute value is calculated to obtain the harmonic measurement.

The following subsections explain the basic operating principles of the phase detector, control loop, and system modeling.

A. Phase Detector

As described in Section IV, VSPT automatically adjusts the sampling frequency to a new value so as to maintain a null error between $\varphi_{\text{ref}}(n)$ and $\varphi_u(n)$. This phase error is estimated by means of a phase detector.

For the special case of $k = 1$ the $\varphi_m(n)$ signal [(8)] is equal to $\varphi_{\text{ref}}(n)$ [(13)], so the mSDFT algorithm tuned with $k = 1$ is used as a phase detector. In fact, only the imaginary part of the mSDFT algorithm is used to obtain the phase error signal ($e_\varphi(n)$) needed for the VSPT technique to adjusts the sampling frequency, as it is demonstrated below.

Under the assumption of a distorted input signal, the voltage grid can be represented as follows:

$$x(n) = \hat{V}_1 \cos[\varphi_u(n)] + \sum_{k=2}^{\infty} \hat{V}_k \cos[k\varphi_u(n) + \phi_k]. \quad (14)$$

The first term represents the grid voltage fundamental component while the second term, the sum of the utility harmonics components, where $\hat{V}_1$ and $\varphi_u(n)$ are the fundamental peak amplitude and utility phase, respectively, and $\hat{V}_k$ and ϕ_k are the peak amplitude and initial phase of the kth harmonics, respectively. This signal is processed by mSDFT tuned with $k = 1$, as seen in Fig. 1(b). Then, the imaginary part of (7) becomes an oscillating signal generated by the multiplication between (14) and the imaginary part of the twiddle factor

$$\begin{aligned}\text{Im}\{x^*(n)\} = x(n)\sin(\varphi_m(n)) &= \frac{\hat{V}_1}{2}\sin[\varphi_m(n) - \varphi_u(n)] \\ &+ \frac{\hat{V}_1}{2}\sin[\varphi_m(n) + \varphi_u(n)] \\ &+ \sum_{k=2}^{N/2}\frac{\hat{V}_k}{2}\sin[\varphi_m(n) - k\varphi_u(n) - \phi_k] \\ &+ \sum_{k=2}^{N/2}\frac{\hat{V}_k}{2}\sin[\varphi_m(n) + k\varphi_u(n) + \phi_k]. \quad (15)\end{aligned}$$

As shown in (15), any sinusoidal signal in the voltage grid generates two terms. The first one has a phase equal to the difference of the modulated sequence phase and the analyzed signal phase. The second term, in turn, is equal to the sum of both phases.

The digital notch filter of (6) rejects the oscillating signals from $\text{Im}[x^*(n)]$ by placing zeros in the grid frequency multiples of the transfer function. This process results in the imaginary component of the $k = 1$-bin

$$\text{Im}\{\tilde{X}_1(n)\} = \frac{\hat{V}_1 N}{2}\sin[\varphi_m(n) - \varphi_u(n)] \quad (16)$$

where N is the gain of the filter (Fig. 2). If the phase difference between $\varphi_m(n)$ and $\varphi_u(n)$ is assumed to be very small in (16), the sine function can be approximated by this argument

$$\text{Im}\{\tilde{X}_1(n)\} \approx K_m N[\varphi_m(n) - \varphi_u(n)] \quad (17)$$

where K_m is equal to the factor $\hat{V}_1/2$. The difference between $\varphi_m(n)$ and $\varphi_u(n)$ is the phase error of the system $e_\varphi(n)$. Then (17) is the system error signal ($e_r(n)$) which is proportional to $e_\varphi(n)$

$$e_r(n) = K_m N e_\varphi(n). \quad (18)$$

The use of mSDFT in this manner allows in obtaining an error signal proportional to the phase error of the system with the substantial advantage of its simple structure. The ability to reject oscillations in the $e_\varphi(n)$ signal enhances the robustness of the phase error detection method adopted.

B. Control Loop

The aim of this section is to obtain a mathematical model of the proposed system to design the system controller ($G_c(z)$) and achieve the required system response. To model the system, the samples are handled as a sequence with no reference to sampling times. This enables z transform use even in a variable frequency sampling system, such as the one proposed in this manuscript.

The increment of the φ_u phase during the sampling period results from the integral of the input angular frequency during the corresponding sampling period

$$\varphi_u(n+1) = \varphi_u(n) + \int_{t(n)}^{t(n+1)} \omega dt \quad (19)$$

where $t(n)$ and $t(n+1)$ are consecutive sampling times. Assuming that the input frequency remains constant during the sampling period, (19) can be approximated as follows:

$$\varphi_u(n+1) = \varphi_u(n) + \omega T_s(n). \quad (20)$$

The objective of the VSPT is to achieve N equally spaced instants per input cycle under steady-state conditions. Therefore, the phase increment of the modulated sequence (φ_m) between sampling instants should be equal to $2\pi/N$. This sequence can be expressed by the following equation:

$$\varphi_m(n+1) = \varphi_m(n) + \frac{2\pi}{N}. \quad (21)$$

Equations (20) and (21) can be transformed into the z-domain yielding (22) and (23)

$$\varphi_u(z) = \omega T_s(z)\frac{1}{(z-1)} \quad (22)$$

$$\varphi_m(z) = \frac{2\pi}{N}\frac{1}{(z-1)}. \quad (23)$$

Given the fact that mSDFT is used as a phase detector, in the case of a small signal model, the system error signal is defined by (17). This signal is the system phase error affected by the $H_{\text{DNF}}(z)$ transfer function (which rejects all the oscillations from the phase error) and K_m. Then the z-domain expression for the system error is as follows:

$$e_r(z) = K_m H_{\text{DNF}}(z) e_\varphi(z). \quad (24)$$

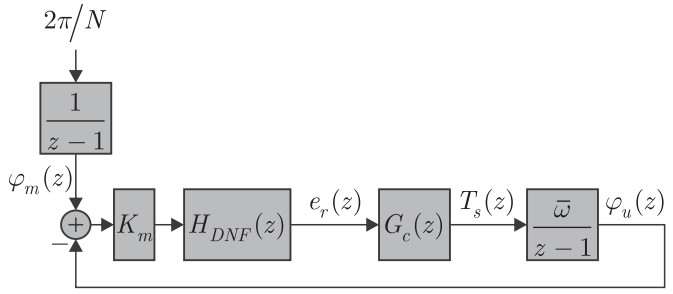

Fig. 5. System model of the proposed method.

This error signal is used to modify the sampling period T_s and to enable $\varphi_u = \varphi_m$ achieve synchronism. The sampling period T_s is a function of the phase error e_φ, and is given by the controller equation

$$T_s(z) = e_\varphi(z) K_m H_{\mathrm{DNF}}(z) G_c(z). \tag{25}$$

From the above equations and linearizing around a center frequency equal to $\bar{\omega} = 2\pi \times 50\,\mathrm{Hz}$, a linear model for the proposed method can be built. The resulting linear model in the z-domain is illustrated in Fig. 5. This model is mathematically identical to that found in [33], so the same strategy for control design can be adopted. However, the bandwidth required for the proposed method is lower than the bandwidth required for the synchronization method cited. As a result, a simpler controller is proposed

$$G_c(z) = K \frac{(z-a)}{(z-1)}. \tag{26}$$

Following the stability analysis from [33], the zero location and gain of the controller shown in (26) are tuned to $a = 0.99745\,(2.6\,\mathrm{Hz})$ and $K = 2.7038 \times 10^{-7}\,(-131.36\,\mathrm{dB})$, respectively. Thereby, a phase margin of 45° and an open-loop crossover frequency of 5.905 Hz are obtained.

For the analyzed application, this simple controller works properly. However, if a faster response in the frequency estimation is needed, a more complex control can be implemented.

C. Efficient Architecture of the Harmonic Measurement System

As mentioned above, there exists mathematical identity between (4) and (12), whereby, regardless of the type of IIR filter implemented, the phase detector and the system model remain valid in both cases. So since only one N-length SW is needed in (12) and the stored values for this are real and not complex, this form of mSDFT is selected for the proposed method. In this manner, a significant memory reduction is attained. Fig. 6 shows the actual and final form of the proposed method.

V. Performance Evaluation

This section studies the performance of the proposed method by means of computer simulations. To this aim, a structure such as that shown in Fig. 6 with $N = 128$ is simulated using Matlab/Simulink software. Several scenarios were evaluated to assess the performance of the proposed method.

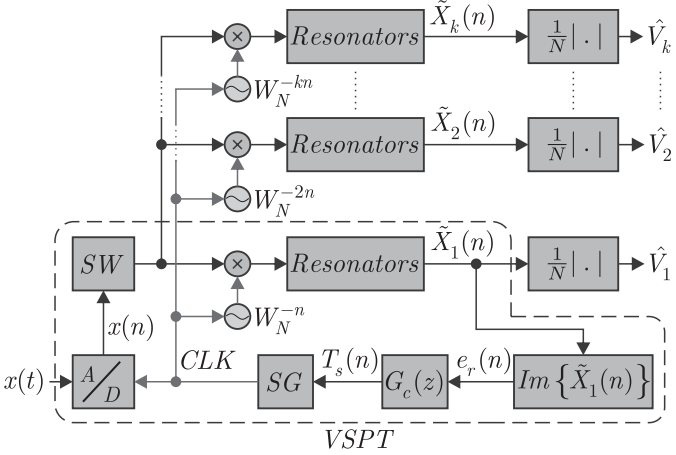

Fig. 6. Scheme of the proposed method.

The input signal to be analyzed by the proposed algorithm is

$$\begin{aligned} x(t) = {} & \sin(w_L t + \phi_1) + 0.2\sin(3w_L t + \phi_3) \\ & + 0.1\sin(5w_L t + \phi_5) + 0.08\sin(9w_L t + \phi_9) \\ & + 0.06\sin(11 w_L t + \phi_{11}) \\ & + 0.04\sin(13 w_L t + \phi_{13}) \end{aligned} \tag{27}$$

where $w_L = 2\pi \times 50\,\mathrm{Hz}$ and the initial phase angles ϕ_k are randomly selected between zero and 2π rad. This signal is chosen particularly for its high content of odd harmonics, typical of weak networks.

For each test performed, the real amplitude (black line) and the estimated amplitude (gray line) of the 1st, 3rd, 5th, 9th, 11th, and 13th harmonics are shown. The values are expressed on a per unit (pu) basis, using the amplitude of the fundamental component in initial conditions as reference. In addition, the frequency of the fundamental component (f_L) is represented by a black line, and the one estimated by the proposed method, by a gray line. The estimated frequency is calculated from the sampling frequency (f_s) and N (i.e., $f_L = f_s/N$).

Two indicators were defined to evaluate the measurement error. One of them, called steady-state error (Δe_{st}), is the value of the maximum deviation of the estimated value from the actual harmonic in steady state. The other, called settling time (t_{set}), is the time between the occurrence of a disturbance and the time when the estimation of the fundamental component ($\hat{V}_1$) settles to 1% error band of V_1 final value. The reason why $\hat{V}_1$ is chosen for determining the settling time is that the measurement of the fundamental component is critical to the frequency adjustment technique which, at the same time, affects the performance of all harmonics estimations. The results of these indicators for all tests are shown in Table II.

A. Amplitude Tracking

To study the method's ability to address variations in harmonics amplitudes, two possible scenarios are simulated. The first simulation studies the effect of the amplitude step-change

TABLE II
SIMULATION TEST RESULTS

k		Fig. 7	Fig. 8	Fig. 9	Fig. 10	Fig. 11
1	Δe_{st}[pu]	0	0.016	0	0.00108	0.0458
3	Δe_{st}[pu]	0	0.005	0	0.000402	0.0155
5	Δe_{st}[pu]	0	0.0035	0	0.000388	0.0104
9	Δe_{st}[pu]	0	0.0025	0	0.000343	0.0067
11	Δe_{st}[pu]	0	0.0018	0	0.000266	0.0058
13	Δe_{st}[pu]	0	0.0014	0	0.000495	0.0049
t_{set}[ms]		20	—	20	20	—

on the method performance. The amplitudes of the input signal harmonics undergo a step-change of 20% of their nominal values in $t = 20$ ms. The estimated values of the amplitudes are shown from Fig. 7(a) to 7(f). In Fig. 7(a), it is shown that V_1 settles to the 1% error band ($\hat{V}_1 \in [1.188, 1.212]$) in 20 ms, and, at the same time, all measurements are settled. The proposed scheme can track step changes in amplitudes with zero error in all harmonic components under a steady-state condition. Since the adjustment of the sampling frequency is conducted with $\mathrm{Im}\{\tilde{X}_1(n)\}$ estimation, when the step-change occurs in this harmonic, an oscillatory transient appears in the estimated frequency. This decaying oscillatory transient has a maximum peak error of less than 0.15 Hz, and then settles down to the actual value with zero error in steady state [Fig. 7(g)]. This transient in $\hat{f}_L$ has a small effect on amplitude estimations, as seen from Fig. 7(a) to (f).

The second simulation concerns the study of the method performance in tracking slow variations in V_k. The amplitude of each harmonic component changes from its nominal value of V_k to $V_k + 0.2V_k \sin(2\pi t + \delta_k)$ (δ_k is chosen for the worst case) at $t = 0.2$ s. The steady-state oscillations present in both, the estimated frequency, and the measured harmonics are due to the continuous variations in the harmonic signal amplitudes, i.e., the input signal ceases to be stationary. For this reason, the accuracy of any DFT-based technique is reduced. Fig. 8(a)–(f) shows that the proposed method accurately tracks the 1 Hz amplitude variations with a delay of 10 ms in the worst case. The settling time is not shown in the table because the error in the measurement of $\hat{V}_1$ is not bounded to 1%, even so steady-state errors remain within reasonable limits (Table II). Fig. 8(g) shows the estimated frequency, where the oscillatory behavior can be noticed. These oscillations are produced by the continuous variation of $\mathrm{Im}\{\tilde{X}_1(n)\}$, which prevents the exact adjustment of the sampling frequency. In the transient, the peak error is about 0.156 Hz and, in steady state, the maximum variation is less than 0.01 Hz. In this case, the frequency error remains bound well below 1%. Yet, even under these conditions, the error indicators remain within acceptable ranges, as shown in Table II.

B. Frequency Tracking

The ability of the method to measure harmonics in situations where the frequency deviates from its nominal value is evaluated by simulating two possible scenarios. The first simulation analyzes the effect of a frequency step of −0.5 Hz

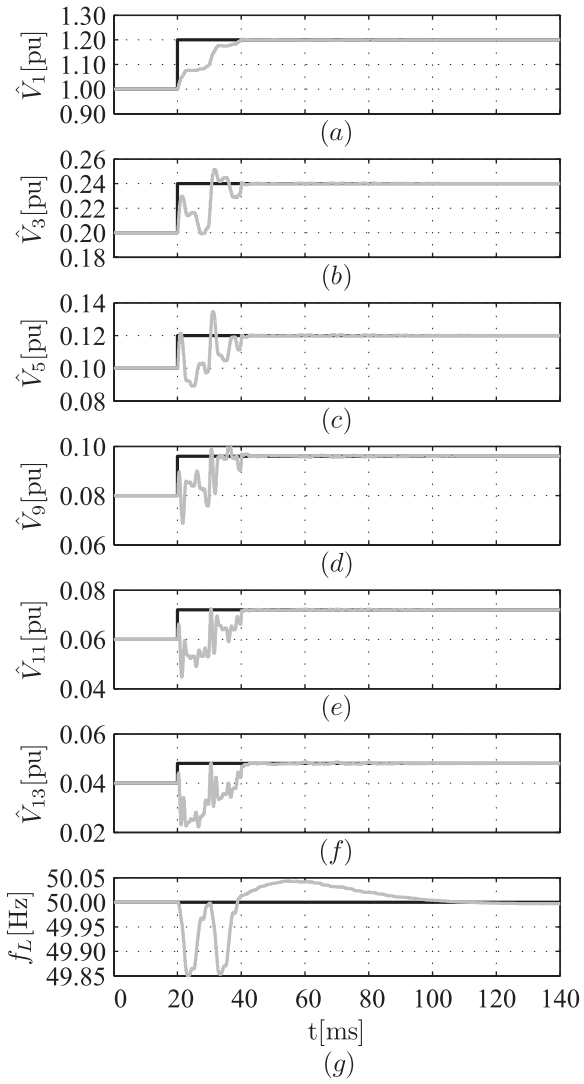

Fig. 7. Performance of the proposed method for harmonics undergoing a 20% step-change in their amplitudes nominal values. (a)–(f) Extracted amplitude of the k-harmonics (gray) and its actual value (black). (g) Estimated fundamental frequency (gray) and its actual value (black).

on the performance of the proposed method. This step-change is imposed at $t = 0.1$ s. Fig. 9(a)–(f) shows the effect of the frequency step-change on the estimated harmonic amplitudes. During the transient, an oscillatory behavior is noticed. These oscillations are attributed for two reasons: one of them is the high distortion of the analyzed signal and the other is the incorrect frequency estimation because of singularities which are not located exactly at multiples of the current line frequency (f_L). Despite this, even during the transient, the maximum error in the measurement of $\hat{V}_k$ does not exceed 0.005 pu. The settling time for this scenario is 20 ms (Table II). Variations in the estimated values are extinguished once the sampling frequency is properly adjusted by the method. Fig. 9(g) shows the frequency tracking feature that accurately tracks steps in frequency. After 4 ms, the frequency error remains below the 1% limit with a maximum error in the transient of 0.5 Hz. Then, under a steady-state condition, the system achieves null error in the estimation of the fundamental frequency.

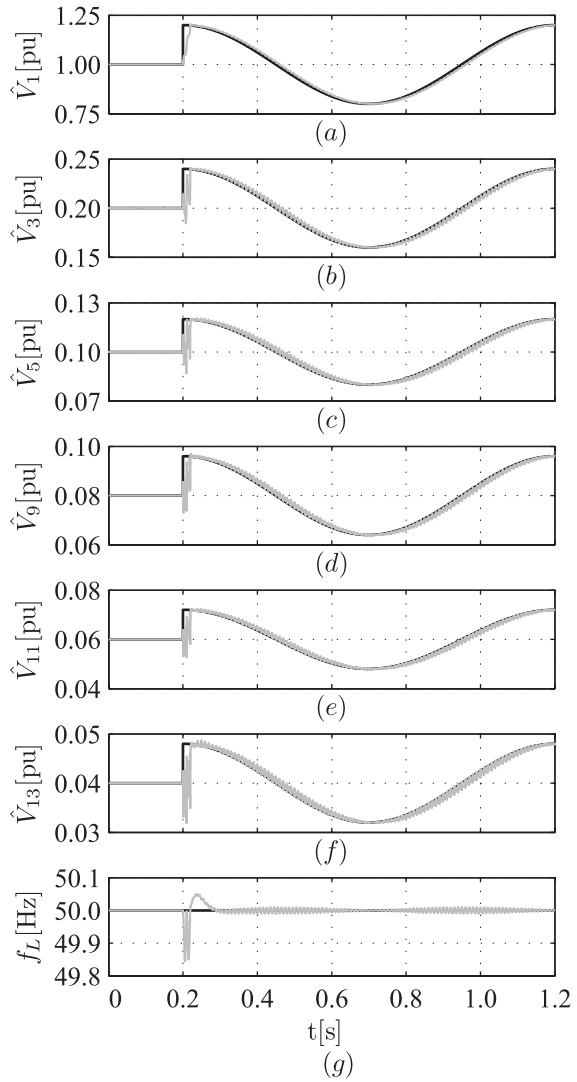

Fig. 8. Performance of the proposed method for extracting harmonics of oscillatory amplitudes. (a)–(f) Extracted amplitude of the k-harmonics (gray) and its actual value (black). (g) Estimated fundamental frequency (gray) and its actual value (black).

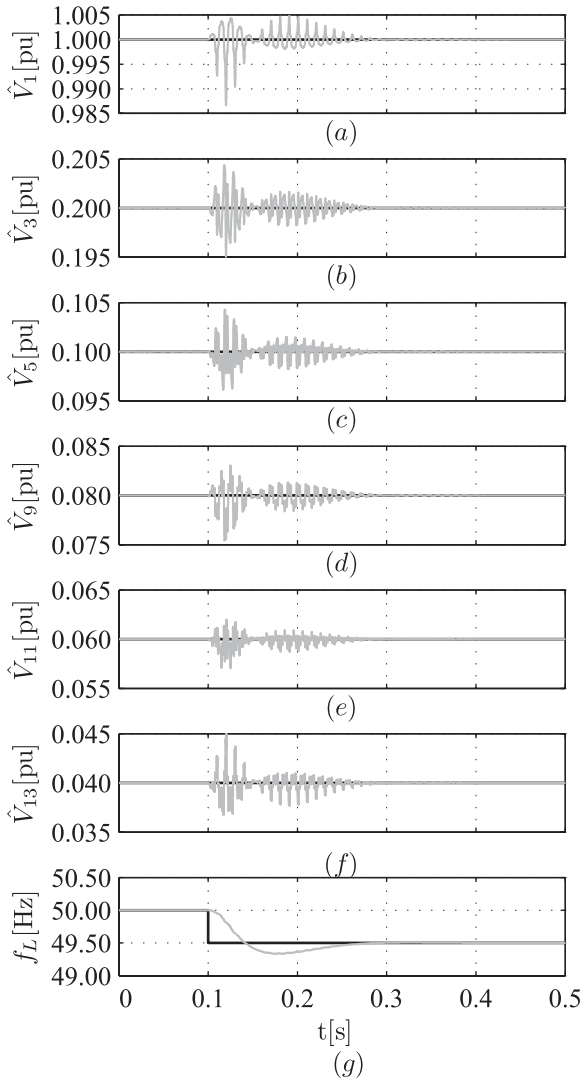

Fig. 9. Performance of the proposed method extracting the harmonics undergoing a step-change in the fundamental frequency. (a)–(f) Extracted amplitude of the k-harmonics (gray) and its actual value (black). (g) Estimated fundamental frequency (gray) and its actual value (black).

The aim of the second simulation is to verify the method performance when a periodic and continuous frequency variation occurs. To achieve that, an oscillatory variation in the fundamental frequency of the input signal (27) is added. The fundamental frequency changes from its nominal value of 50 Hz to $50 + 0.5\sin(2\pi t + \psi)$ Hz at $t = 0.2$ s (ψ is chosen for the worst case). Fig. 10(a)–(f) shows the response of the system to a continuous variation of the fundamental frequency. During the transient, the estimations have a small peak error and, in steady state, the oscillatory fundamental frequency causes oscillations in the estimated magnitudes. These oscillations are attributed to the continuous variation of the fundamental frequency, which prevents the exact adjustment of the sampling frequency, and therefore reduces the disturbances rejection of $H_{\mathrm{DNF}}(z)$ [(6)]. After a settling time of 20 ms, the error in the measurement of $\hat{V}_1$ is bounded below 1%. In addition, in steady state, the error remains bound within acceptable margins (Table II). Actual and estimated frequency values are shown in Fig. 10(g). A maximum error of 0.5 Hz is obtained during the transient. Then, in steady state, the estimated frequency reaches the actual frequency, following its variations with a delay of 4 ms and a maximum peak error of 0.0375 Hz. A detailed analysis of the error indicators for both tests and for all harmonics can be found in Table II.

Frequency variations are common in utility networks due to the power imbalance between the generation and load demand. Then, the results of these trials test the robustness of the method in such cases, making it an attractive technique.

C. Simultaneous Tracking

A more challenging measurement scenario is also considered in which the test signal (27) undergoes simultaneous variations of both frequency and amplitude. The fundamental frequency changes from its nominal value of 50 Hz to $50 + 0.5\sin(2\pi t + \psi)$ Hz at $t = 0.2$ s (ψ is chosen for the worst case), and at the same time the amplitudes start to oscillate as $V_k + 0.2V_k\sin(6\pi t + \delta_k)$ (δ_k are chosen for

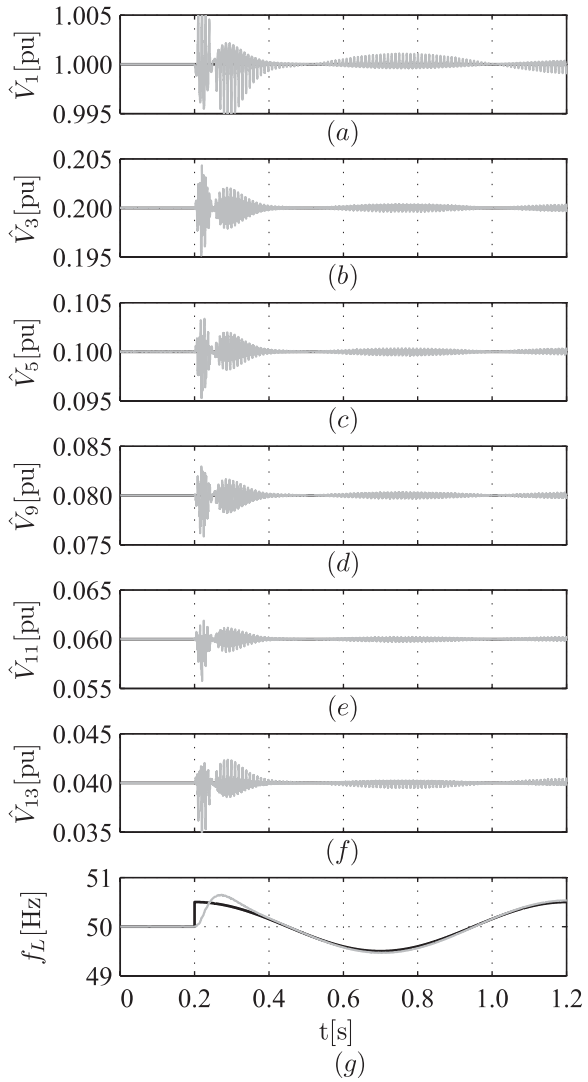

Fig. 10. Performance of the proposed method for extracting the harmonics of the signal with oscillating fundamental frequency. (a)–(f) Extracted amplitude of the k-harmonics (gray) and its actual value (black). (g) Estimated fundamental frequency (gray) and its actual value (black).

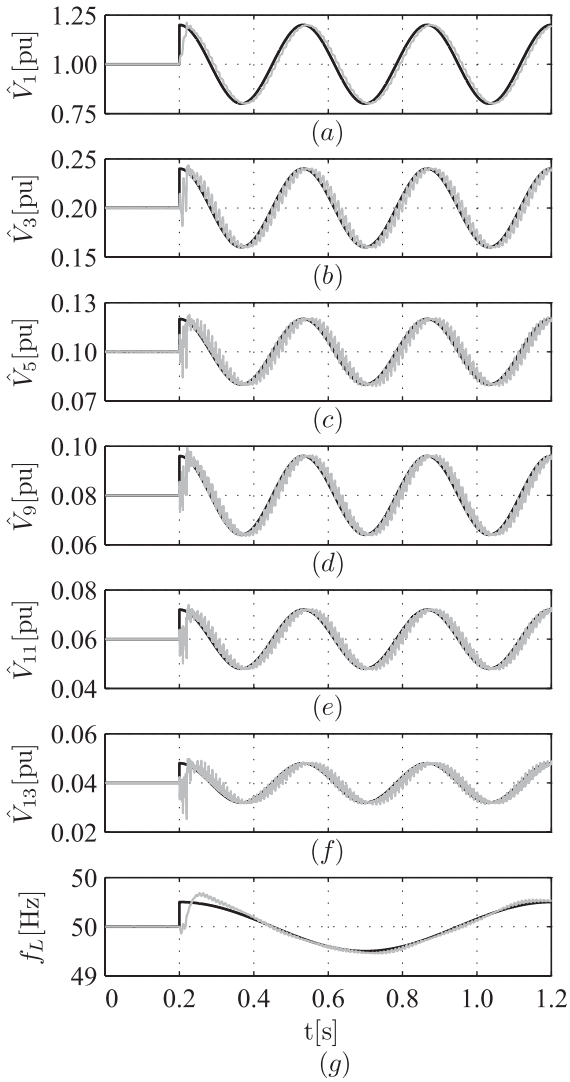

Fig. 11. Performance of the proposed method for extracting harmonics of oscillatory amplitudes with oscillating fundamental frequency. (a)–(f) Extracted amplitude of the k-harmonics (gray) and its actual value (black). (g) Estimated fundamental frequency (gray) and its actual value (black).

the worst case). This scenario, where the amplitude varies at a rate of 3 Hz combined with a frequency variation rate of 1 Hz is a very demanding situation, although it should be noted that in practice this is unlikely to happen due to the dynamics imposed by power grids. The estimated amplitudes for this scenario are shown from Fig. 11(a) to (f). The proposed scheme tracks amplitude variations with a delay of about 10 ms in the worst case. Fig. 11(g) shows that the proposed scheme tracks variation in the fundamental frequency, with moderated oscillation over the nominal value, and a maximum error in steady state of 0.09 Hz. The settling time for this case is not shown in the table because the error in the measurement of $\hat{V}_1$ is not bounded to 1%, even so the method performance is satisfactory. The errors of the estimated frequency and the harmonic measurement are the largest obtained among the trials conducted. This is due to the fact that amplitude variations are faster. However, even in this unlikely situation, the system is stable and errors in steady state are acceptable (Table II).

The performance evaluation of the proposed algorithm proves that the method is able to track variations in power signal characteristics, such as time variations of harmonics amplitudes and fundamental frequency. Unavoidable oscillations and delays in the estimated frequency and extracted amplitudes occur, though within an acceptable range, making the method applicable to most practical cases.

D. Noise Rejection

Performance of proposed method working in the presence of noise is discussed in this section. Accordingly, a white Gaussian noise is added to the test signal showed in (27) yielding a signal to noise rate (SNR) of 30 dB. Also two disturbances are added to the test signal to evaluate the noise influence during transients. Fig. 12 shows the response of the method for this scenario, wherein the amplitudes undergo a step-change of 20% of their nominal values in $t = 0.25$ s

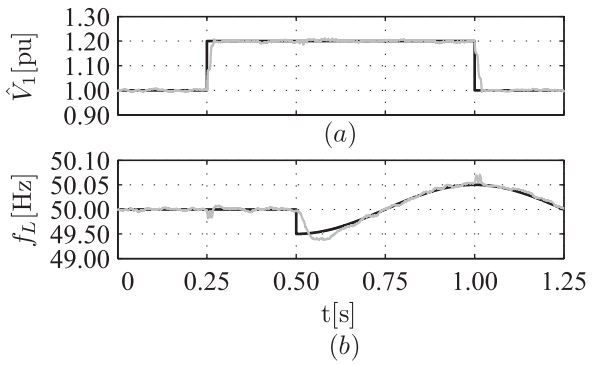

Fig. 12. Performance of the proposed method for extracting the harmonics of the signal with a SNR= 30 dB. (a) Estimated (gray) and real (black) fundamental amplitude. (b) Estimated (gray), and real (black) grid frequency.

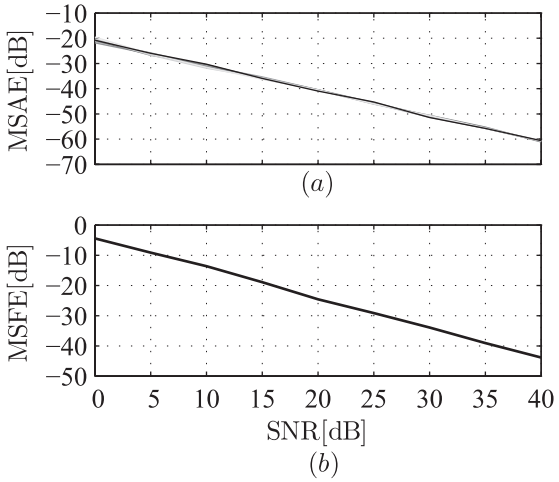

Fig. 13. (a) Mean square amplitude error in decibels for several SNR, within a time window of 10 s. (b) Mean square frequency error in decibels for several SNR, within a time window of 10 s.

and the fundamental frequency changes from its nominal value to $50 + 0.5\sin(2\pi t + \psi)$ Hz at $t = 0.5$ s. A comparison between this figure and tests performed in Figs. 7 and 10, allows concluding that dynamic response remains unchanged.

Finally, the test signal in (27) was degraded with white Gaussian noise for different levels of SNR, to study the performance of the system in steady-state condition. Fig. 13(a) shows the mean square amplitude error (MSAE) in decibels ($10\log_{10}$(MSAE)) for all estimated amplitudes in relation to different SNR levels, calculated during a time window of 10 s. The estimations are grouped practically on the same curve, so the noise has an equal effect on the harmonics measurement method. The mean square frequency error (MSFE) in decibels ($10\log_{10}$(MSFE)) is shown in Fig. 13(b). Both indicators are monotonically decreasing and, even in the worst case of SNR, the method performed well.

VI. Implementation

Owing to the method modular nature (Fig. 6), the small number of mathematical operations required, and the simplicity of the control loop, the proposed method is more than suitable for implementation in an FPGA platform. The algorithm is implemented in a Spartan-3E xc3s1600e FPGA device from Xilinx. The frequency of the FPGA clock is of 50 MHz, which means that the sampling period has a resolution of 20 ns. Logic synthesis, place and route, and timing analyses are performed using ISE Design Suite ver.13 design tool. A full explanation of the implementation can be found in [35], from which the key information is extracted and presented below. The use of resources based on hierarchy can be seen in Table III. The complex resonator component includes two resonators and two multipliers from Fig. 6 (for calculation of the real and imaginary part of the desired spectral component). It should be noticed that if M harmonics is intended to be measured, the absolute value and complex resonator sections must be repeated M times. The resources used for the FPGA implementation allow to implement the harmonics measurement algorithm as part of a more complex system. It is worth noticing that the nominal frequency in which this design operates ($50\,\text{Hz} \times 128 = 6.4\,\text{kHz}$) is lower than the maximum frequency registered by the analysis of each individual component.

TABLE III
Resource Usage by Component

Component	f_{max}[MHz]	Consumed Resource		
		Slices	FF's	LUT's
Sliding Window	221.926	98	95	195
Twiddle Factors	93.897	453	232	777
VSPT	128.231	188	278	209
Complex Resonator	190.186	104	190	68
Absolute Value	90.158	604	721	864

A. Timing Versus Area

Oftentimes in the design of any system to be implemented in an FPGA platform the designer needs to make a tradeoff between timing performance and area consumption. Sometimes the system is part of a larger system contained in the same device, so certain area constraints need to be met. On other occasions, the area is not an issue and a key factor is timing performance.

The proposed method can meet both requirements given its high implementation flexibility. If it were necessary to reduce the consumption area, this could be attained by generating only one mSDFT component and one absolute value component, rather than several for each harmonics, a finite state machine (FSM) to reuse the component and a RAM to store the important values, the method can be implemented with a significant reduction in area consumption. Conversely, if the aim was to obtain the measurement as fast as possible, this could be achieved by repeating the components previously mentioned for each harmonics that is to be measured.

Final implementation is determined by application specification, the designer criterion, and not by the method itself.

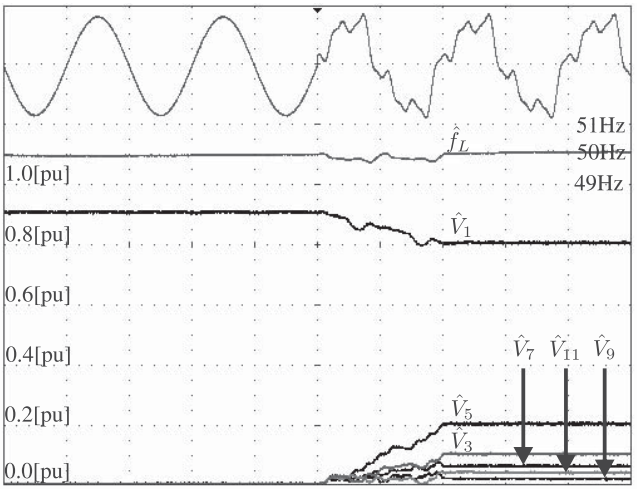

Fig. 14. Online amplitude tracking. Time scale is 10 ms/div.

B. Experimental Testing

This section presents the experimental results obtained from the implementation of the proposed method as shown in Section VI. A test signal with known harmonic content was used to quantify the performance of the proposed method; and to conduct the experimental trial, a test bench comprising several devices was used, where three parts can be differentiated: generation, sampling and processing, and visualization. A Hewlett Packard 33120A programmable waveform generator was employed to generate the test signal; and to sample and process the measurement, an AD677 with an FPGA Spartan-3E xc3s1600e was used. Finally, a Tektronik MSO 2024 oscilloscope was used to visualize and process the signals of interest. The test signal used changed from an ideal sinusoidal waveform to a nonideal one, thus time response and precision could be measured. The fundamental component changed from 0.9[pu] to 0.8[pu], and then 0.1[pu] of 3rd, 0.2[pu] of 5th, 0.04[pu] of 7th, 0.02[pu] of 9th and 0.06[pu] of 11th harmonics were added. Values are expressed on a per unit (pu) basis, using a maximum generator voltage of 18 V peak-to-peak as reference. The test signal, the estimated frequency (f_L), and the estimated amplitude of the fundamental, as well as the 3rd, 5th, 7th, 9th, and 11th harmonics ($M = 6$) are shown in Fig. 14. The test demonstrates that the measurements are stabilized in one cycle of the input signal. After this transient, the measurements present neither oscillations NOR variations. The frequency estimation ($\hat{f}_L$) remains within the 1% frequency error band in the transient, and, after one cycle, it settles to 50 Hz.

Tables IV and V show a comparison between harmonics measurements done with the proposed method and an FFT performed with the MSO 2024, both for ideal and distorted conditions. For the proposed method, the mean (μ) and standard deviation (σ) of each estimated harmonic in a period of one second are presented. All values are in volts rms.

Finally, a measurement of total harmonics distortion (THD) of the grid voltage during a whole day is presented in Fig. 15. To calculate the THD index, the necessary components for estimating the first 40 grid harmonics have been implemented ($M = 40$). The analyzed grid belongs to a university research laboratory and a marked increase in the THD index is observed from 8:00 A.M. to 4:00 P.M. As evidenced in this paper, the proposed method allows for the analysis of power quality in real grids with good response.

TABLE IV
MEASUREMENT COMPARATIVE FOR IDEAL CONDITION, WHERE ALL VALUES ARE IN VOLTS rms

	V_k	FFT	Proposed Method	
			μ	$\sigma[10^{-3}]$
$\hat{V}_1$	5.7276	5.78125	5.77311	0.5547437
$\hat{V}_3$	0	0.00281	0.00068	0.4001204
$\hat{V}_5$	0	0.00281	0.00109	0.4987732
$\hat{V}_7$	0	0.00000	0.00436	0.7015291
$\hat{V}_9$	0	0.00562	0.00274	0.5157773
$\hat{V}_{11}$	0	0.00281	0.00075	0.4253181
$\text{THD}_{\%}$	0	0.129	0.177	4.9049102

TABLE V
MEASUREMENT COMPARATIVE FOR DISTORTED CONDITION, WHERE ALL VALUES ARE IN VOLTS rms

	V_k	FFT	Proposed Method	
			μ	$\sigma\ [10^{-3}]$
$\hat{V}_1$	5.0912	5.14156	5.13152	0.5571616
$\hat{V}_3$	0.6364	0.62500	0.64020	0.4323879
$\hat{V}_5$	1.2728	1.27594	1.28287	0.5333326
$\hat{V}_7$	0.2546	0.24281	0.25319	0.6858771
$\hat{V}_9$	0.1273	0.13875	0.12951	0.4511063
$\hat{V}_{11}$	0.3818	0.38750	0.38490	0.7254746
$\text{THD}_{\%}$	29.4746	29.155	29.455	11.7238594

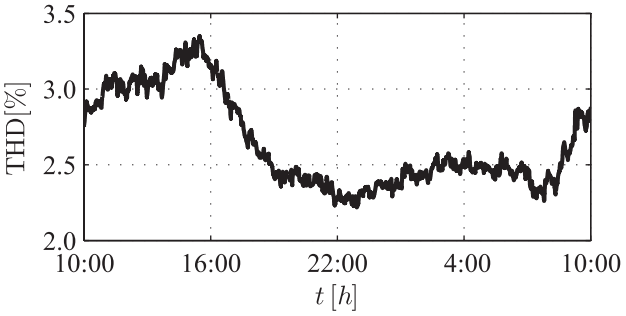

Fig. 15. Grid total harmonics distortion (THD) estimated by the proposed method.

VII. INTERHARMONICS AND SUBHARMONICS

As it was shown in previous sections, the VSPT is able to obtain a sampling frequency multiple of the input frequency regardless of the number of harmonics and their amplitude. This is possible due to the rejection that mSDFT tuned with $k = 1$ imposes to the nonfundamental components of the input signal. However, the proposed method, as shown so far, does not reject subharmonics and interharmonics. When the input signal is distorted by this kind of components, the

estimated amplitude and sampling period present oscillations in steady state. On the other hand, it is important to note that the VSPT stability is not affected by subharmonics and inteharmonics, since they are only disturbances on the control loop. Steady-state error depends on the distorted amplitude and loop rejection but, considering that the fundamental amplitude is bigger than other components, the error is within acceptable limits.

As it was previously stated, the proposed method presents high implementation flexibility. The problem described in the previous paragraph can be solved by increasing SW length and maintaining the rest of the structure unchanged (with the exception of controller coefficients which have to be recalculated). By doing this, DFT resolutions and rejection of subharmonics and interharmonics are increased while estimation of these components is allowed. For example, a resolution of 25 Hz is obtained with a double length of SW, therefore, subharmonics and interharmonics close to multiples of 25 Hz are highly attenuated. The IEC61000 standard imposes a DFT measurement of the input signal in a time window corresponding to a 10-grid period [12], [13]. Therefore, an SW of ten times greater length can be adopted. Nevertheless, it is important to note that there is a tradeoff between mSDFT resolution and speed convergence.

VIII. Conclusion

A new method for harmonic measurement is presented in this paper. The method uses the mSDFT algorithm to calculate the grid harmonic content, with no errors or potential instabilities, due to finite precision representation. Moreover no damping factor is needed. The sampling frequency is automatically adjusted to be an integer multiple of the line frequency, thereby avoiding spectral leakage and picket–fence effects, well-known problems affecting DFT-based techniques.

Several scenarios of possible operating conditions were simulated. This study shows that the proposed method is robust and accurate even in time-varying conditions. The performance for noisy signals was presented, and for the different SNR, the results are considered reasonable for practical applications.

The system implementation is conducted in an FPGA platform obtaining a flexible and portable project. The modular nature of the method allows designers to optimize area consumption or timing depending on the project requirements. In this paper, the project is implemented for optimum time response, nonetheless the resources used for FPGA implementation are acceptable, and allow the method to be part of a more complex system.

The performance of the proposed method has been evaluated in several disturbance scenarios. Experimental and simulation results have demonstrated the method measurement capability, even in the case of highly distorted environments, noise degraded signal, and time-varying conditions.

References

[1] M. Bollen and I. Gu, *Signal Processing of Power Quality Disturbances*. New York, NY, USA: Wiley, 2006.

[2] S. Chattopadhyay, *Electric Power Quality*. New York, NY, USA: Springer-Verlag, 2011.

[3] J. Arrillaga and N. Watson, *Power System Harmonics*. New York, NY, USA: Wiley, 2003.

[4] A. Girgis and F. Ham, "A quantitative study of pitfalls in the FFT," *IEEE Trans. Aerosp. Electron. Syst.*, vol. 16, no. 4, pp. 434–439, Jul. 1980.

[5] I. Santamaria-Caballero, C. Pantaleon-Prieto, J. Ibanez-Diaz, and E. Gomez-Cosio, "Improved procedures for estimating amplitudes and phases of harmonics with application to vibration analysis," *IEEE Trans. Instrum. Meas.*, vol. 47, no. 1, pp. 209–214, Feb. 1998.

[6] X. Dai and R. Gretsch, "Quasi-synchronous sampling algorithm and its applications," *IEEE Trans. Instrum. Meas.*, vol. 43, no. 2, pp. 204–209, Apr. 1994.

[7] V. Jain, W. L. Collins, and D. C. Davis, "High-accuracy analog measurements via interpolated FFT," *IEEE Trans. Instrum. Meas.*, vol. 28, no. 2, pp. 113–122, Jun. 1979.

[8] T. Grandke, "Interpolation algorithms for discrete Fourier transforms of weighted signals," *IEEE Trans. Instrum. Meas.*, vol. 32, no. 2, pp. 350–355, Jun. 1983.

[9] G. Andria, M. Savino, and A. Trotta, "Windows and interpolation algorithms to improve electrical measurement accuracy," *IEEE Trans. Instrum. Meas.*, vol. 38, no. 4, pp. 856–863, Aug. 1989.

[10] D. Agrez, "Weighted multipoint interpolated DFT to improve amplitude estimation of multifrequency signal," *IEEE Trans. Instrum. Meas.*, vol. 51, no. 2, pp. 287–292, Apr. 2002.

[11] D. Gallo, R. Langella, and A. Testa, "Desynchronized processing technique for harmonic and interharmonic analysis," *IEEE Trans. Power Delivery*, vol. 19, no. 3, pp. 993–1001, Jul. 2004.

[12] *Electromagnetic Compatibility (EMC) Part 3-2*, IEC Standard 61000-3-2, Aug. 2000.

[13] *Electromagnetic Compatibility (EMC) Part 3-4*, IEC Standard 61000-3-4, Oct. 1998.

[14] E. Jacobsen and R. Lyons, "The sliding DFT," *IEEE Signal Process. Mag.*, vol. 20, no. 2, pp. 74–80, Mar. 2003.

[15] J. F. Chicharo and M. T. Kilani, "A sliding Goertzel algorithm," *Signal Process.*, vol. 52, no. 3, pp. 283–297, 1996.

[16] H. Ma and A. Girgis, "Identification and tracking of harmonic sources in a power system using a Kalman filter," *IEEE Trans. Power, Delivery*, vol. 11, no. 3, pp. 1659–1665, Jul. 1996.

[17] A. Girgis, W. Chang, and E. Makram, "A digital recursive measurement scheme for online tracking of power system harmonics," *IEEE Trans. Power Delivery*, vol. 6, no. 3, pp. 1153–1160, Jul. 1991.

[18] J. Macias and A. Gomez-Exposito, "Self-tuning of Kalman filters for harmonic computation," *IEEE Trans. Power Delivery*, vol. 21, no. 1, pp. 501–503, Jan. 2006.

[19] M. H. J. Bollen, I.-H. Gu, S. Santoso, M. McGranaghan, P. Crossley, M. Ribeiro, *et al.*, "Bridging the gap between signal and power," *IEEE Signal Process. Mag.*, vol. 26, no. 4, pp. 12–31, Jul. 2009.

[20] H. C. So, "A comparative study of three recursive least-squares algorithms for single-tone frequency tracking," *Signal Process.*, vol. 83, no. 9, pp. 2059–2062, Sep. 2003.

[21] M. Bettayeb and U. Qidwai, "Recursive estimation of power system harmonics," *Electr. Power Syst. Res.*, vol. 47, no. 2, pp. 143–152, Oct. 1998.

[22] S. Jain, P. Agrawal, and H. Gupta, "Fuzzy logic controlled shunt active power filter for power quality improvement," *IEE Proc. Electr. Power Appl.*, vol. 149, no. 5, pp. 317–328, Sep. 2002.

[23] J. Vazquez and P. Salmeron, "Active power filter control using neural network technologies," *IEE Proc. Electr. Power Appl.*, vol. 150, no. 2, pp. 139–145, Mar. 2003.

[24] L. H. Tey, P. So, and Y. Chu, "Improvement of power quality using adaptive shunt active filter," *IEEE Trans. Power Delivery*, vol. 20, no. 2, pp. 1558–1568, Apr. 2005.

[25] S. Jain and S. Singh, "Exact model order esprit technique for harmonics and interharmonics estimation," *IEEE Trans. Instrum. Meas.*, vol. 61, no. 7, pp. 1915–1923, Jul. 2012.

[26] S. Jain and S. Singh, "Fast harmonic estimation of stationary and time-varying signals using EA-AWNN," *IEEE Trans. Instrum. Meas.*, vol. 62, no. 2, pp. 335–343, Feb. 2013.

[27] S. Luo and Z. Hou, "An adaptive detecting method for harmonic and reactive currents," *IEEE Trans. Ind. Electron.*, vol. 42, no. 1, pp. 85–89, Feb. 1995.

[28] K. Duda, "Accurate, guaranteed stable, sliding discrete Fourier transform [DSP tips & tricks]," *IEEE Signal Process. Mag.*, vol. 27, no. 6, pp. 124–127, Nov. 2010.

[29] E. Jacobsen and R. Lyons, "An update to the sliding DFT," *IEEE Signal Process. Mag.*, vol. 21, no. 1, pp. 110–111, Jan. 2004.

[30] R. G. Lyons, *Streamlining Digital Signal Processing: A Tricks of the Trade Guidebook*. New York, NY, USA: Wiley, 2007.

[31] J.-H. Kim and T.-G. Chang, "Analytic derivation of the finite wordlength effect of the twiddle factors in recursive implementation of the sliding-DFT," *IEEE Trans. Signal Process.*, vol. 48, no. 5, pp. 1485–1488, May 2000.
[32] S. Maestri, P. Donato, R. Petrocelli, I. Carugati, D. Carrica, and M. Benedetti, "Synchronization method for three phase applications," *Int. Rev. Electr. Eng.*, vol. 5, no. 4, pp. 1728–1735, Aug. 2010.
[33] I. Carugati, S. Maestri, P. Donato, D. Carrica, and M. Benedetti, "Variable sampling period filter PLL for distorted three-phase systems," *IEEE Trans. Power Electron.*, vol. 27, no. 1, pp. 321–330, Jan. 2012.
[34] I. Carugati, P. Donato, S. Maestri, D. Carrica, and M. Benedetti, "Frequency adaptive PLL for polluted single-phase grids," *IEEE Trans. Power Electron.*, vol. 27, no. 5, pp. 2396–2404, May 2012.
[35] C. Orallo, I. Carugati, P. Donato, and S. Maestri, "Harmonics measurement with a modulated sliding DFT algorithm on an FPGA platform," in *Proc. EAMTA*, Aug. 2012, pp. 40–46.

Carlos M. Orallo was born in Argentina in 1982. He received the B.S. degree in electronics engineering from Universidad Nacional de Mar del Plata, Mar del Plata, Argentina, in 2011, where he is currently pursuing the Ph.D. degree in electronics.

His current research interests include harmonics measurement, power quality, and signal processing.

Ignacio Carugati was born in Argentina in 1983. He received the B.S. and Ph.D. degrees in electronics engineering from Universidad Nacional de Mar del Plata, Mar del Plata, Argentina, in 2008 and 2012, respectively.

He is currently with Universidad Nacional de Mar del Plata. His current research interests include control systems, power quality, and digital signal processing.

Dr. Carugati is a member of the Consejo Nacional de Investigaciones Cientificas y Tecnicas, Argentina.

Sebastian Maestri was born in Argentina in 1978. He received the Electronics Engineering degree from the National University of Mar del Plata, Mar del Plata, Argentina, in 2005, and the Ph.D. degree in electronics from the University of Mar del Plata, Mar del Plata, in 2009.

He was with the European Laboratory for Particle Physics, Centre Europeene pour la Recherche Nucleaire, Geneva, Switzerland, in control methods for improving the performance of thyristorized power supplies for bending-magnets. He is with the University of Mar del Plata. His current research interests include power electronics, control systems and synchronism methods.

Dr. Maestri is a member of the Consejo Nacional de Investigaciones Cientificas y Tecnicas, Argentina.

Patricio G. Donato was born in Argentina in 1975. He received the B.S. degree in electronics engineering from Universidad Nacional de la Patagonia San Juan Bosco, Patagonia, Argentina, in 2000, and the Ph.D. degree in electronics from Universidad de Alcal, Alcal de Henares, Spain, in 2005.

He is currently with Universidad Nacional de Mar del Plata, Mar del Plata, Argentina. His current research interests include digital signal processing, power line communications, and synchronism methods.

Dr. Donato is a member of the Consejo Nacional de Investigaciones Cientificas y Tecnicas, Argentina.

Daniel Carrica (M'84–SM'00) was born in Dolores, Argentina, in 1958. He received the B.S. and Ph.D. degrees in electronics engineering from Universidad Nacional de Mar del Plata (UNMDP), Mar del Plata, Argentina, in 1984 and 2006, respectively, and the M.Sc. degree in electronics from Universidad Politecnica de Madrid, Madrid, Spain, in 1992.

He joined the Department of Electronics, UNMDP, in 1984, as a Research Assistant, and he was the Head of the same department from 1994 to 1996. Currently, he is a Full Professor. From 1990 to 1999, he was an Associate Scientific with the European Organization for Nuclear Research, Centre Europeene pour la Recherche Nucleaire, Geneva, Switzerland. His current research interests include motion control and power electronics.

Dr. Carrica was the Chair of the Joint Chapter of Argentine IEEE Section from 2003 to 2004.

Mario Benedetti was born in Italy in 1945. He received the B.S. degree in electronics engineering from Universidad Nacional de La Plata (UNLP), La Plata, Argentina, in 1968.

He was with Laboratorio de Electronica Industrial, Control e Instrumentacion, UNLP, from 1969 to 1983, where he was involved in research on the development of electronic instruments for physics research. From 1989 to 1990, he was a Scientific Associate with European Laboratory for Particle Physics, Centre Europeene pour la Recherche Nucleaire, Geneva, Switzerland. Since 1985, he has been a Full Professor with Universidad Nacional de Mar del Plata, Mar del Plata, Argentina, where he is the Director of the Laboratorio de Instrumentacion y Control. His current research interests include power electronics and electromagnetic interference control.

Mr. Benedetti is a member of the Consejo Nacional de Investigaciones Cientificas y Tecnicas, Argentina.